Modeling and Experimental Evaluation of Single Particle Growth in Syndiotactic Polymerization of Styrene

S. R. Sultan, W. J. N. Fernando & Suhairi A. Sata

Journal of Materials Engineering and Performance

ISSN 1059-9495
Volume 22
Number 8

J. of Materi Eng and Perform (2013)
22:2148-2160
DOI 10.1007/s11665-013-0506-2

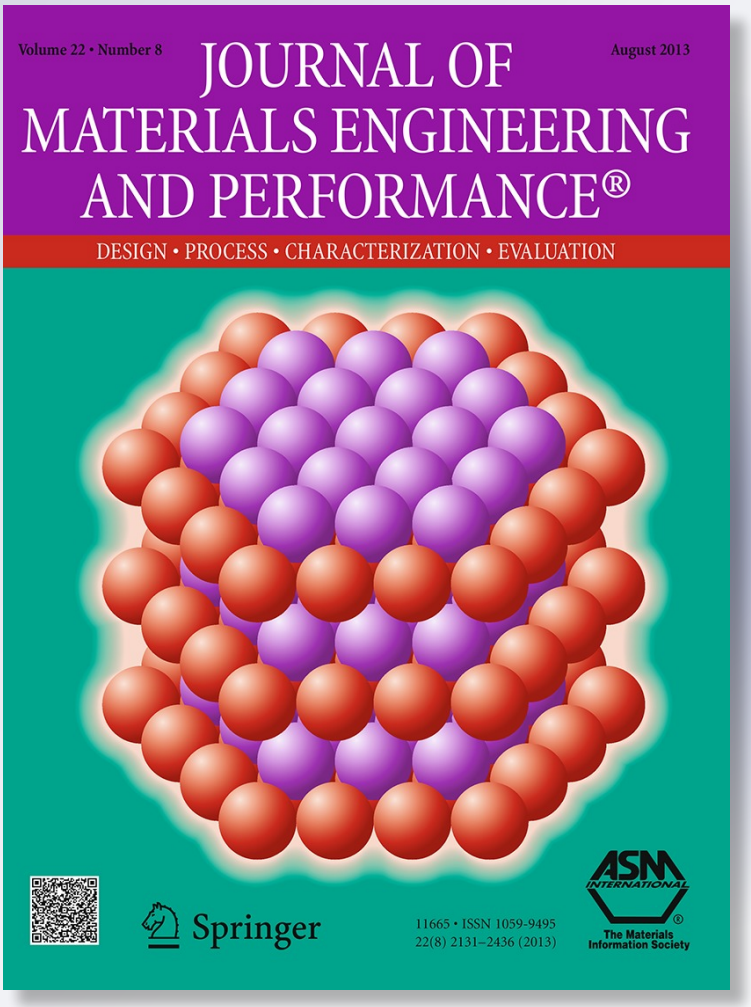

Springer

JMEPEG (2013) 22:2148–2160
DOI: 10.1007/s11665-013-0506-2

1059-9495/$19.00

Modeling and Experimental Evaluation of Single Particle Growth in Syndiotactic Polymerization of Styrene

S.R. Sultan, W.J.N. Fernando, and Suhairi A. Sata

(Submitted December 18, 2012; in revised form February 1, 2013; published online February 22, 2013)

A comprehensive mathematical model and experimental study of single particle growth for styrene polymerization over a silica-supported metallocene catalyst were investigated. The model was developed based on the modification of the well-known multigrain model (MGM) by introducing mesoparticle scale limitations. Thereafter, the model was employed to predict the effects of bulk phase temperature and catalyst properties (initial catalyst active site concentration and initial catalyst particle size) on the polymerization rate, degree of polymerization (DP), and the polydispersity index (PDI) of syndiotactic polystyrene (SPS). The simulation results showed a significant radial distribution of styrene concentration across polymer particle growth at different polymerization conditions. It was found that increasing the initial catalyst concentration and bulk phase temperature resulted in polymerization rate enhancement. In context, the polymerization rate decreased as the initial catalyst particle size increased from 20 to 50 µm. The results revealed that a uniform increase in DP of the polymer was obtained by increasing the initial catalyst concentration and the reaction temperature, while resulting in a decrease of the PDI value. Meanwhile, the DP and PDI values varied inversely under the influence of initial catalyst particle size within a period of time similar to the one needed in the catalyst decay. The simulated results in the study agree well with experimental data of SPS.

Keywords metallocene catalyst, multigrain model, polystyrene, single particle growth, syndiotactic polymerization

1. Introduction

Syndiotactic polystyrene (SPS) is a new polymeric material with high a crystallization rate and a high melting point (270 °C), making this polymer a semicrystalline engineering thermoplastic material with potential industrial applications (Ref 1). SPS was first synthesized by Ishihara (Ref 2) using a soluble titanocene compound, activated by methylalumoxane (MAO). Several styrene polymerizations were carried out with a supported metollocene catalyst, prepared by the reaction of silica gel with MAO and then with a metallocene catalyst (Ref 3-6).

The simplest type of model describes a single catalyst/polymer particle growth based on a spherical layer of polymer particle that is formed around the spherical catalyst particle. Models based on this geometry are commonly called solid core models (SCMs). Monomer diffusion from the polymer shell to the active site on the catalyst surface is the central theme of these models.

Schmeal et al. (Ref 7, 8) and Nagel et al. (Ref 9) used the SCM for olefin polymerization with the aid of heterogeneous Ziegler-Natta catalysts. It was shown that for a single type of active site, this model could not predict broad molecular weight

S.R. Sultan, W.J.N. Fernando, and **Suhairi A. Sata**, School of Chemical Engineering, Universiti Sains Malaysia, 14300 Nibong Tebal, Penang, Malaysia. Contact e-mail: saadraheem76@gmail.com

Nomenclature

$D_{ef,M,i}$	Effective macroparticle diffusivity, at the *i*th grid point (cm^2/min)
$D_{ef,s}$	Effective mesoparticle diffusivity (cm^2/min)
$D_{ef,\mu}$	Effective microparticle diffusivity (cm^2/min)
$D_{m,solv}$	Monomer diffusivity in the solvent (cm^2/min)
k_p	Propagation rate constant (L/(mol h))
k_d	Catalyst deactivation rate constant (h^{-1})
k_s	Liquid film mass transfer coefficient (m^2/s)
$[M]_i$	Monomer concentration in the macroparticle, at the *i*th grid point (mol/L)
$[M]_s$	Monomer concentration in the mesoparticle (mol/L)
$[M]_\mu$	Monomer concentration in the microparticle (mol/L)
$[M]_c$	Monomer concentration at the surface of catalyst fragment (mol/L)
$[M]_b$	Bulk monomer concentration (mol/L)
N	Number of shell
r	Radial position at the macroparticle level (m)
R_c	Radius of catalyst subparticles (m)
R_{N+2}	Macroparticle radius (m)
R_o	Initial catalyst particle radius (m)
$R_{h,i}$	Radius of *i*th hypothetical shells
$R_{p,i}$	Rate of reaction per unit volume at the *i*th grid point (mol/(m^3 s))
$R_{overall}$	Overall time-dependent polymerization rate (g SPS/(g cat h))

Greek Letters

η_s	Mesoparticle diffusion effectiveness factor
η_μ	Microparticle diffusion effectiveness factor
λ_{Lk}	*k*th Moment of live polymers
λ_{Dk}	*k*th Moment of dead polymers

distributions (MWDs). Since the SCM assumes polymerization takes place only on the external surface of the catalyst, average properties of all polymer chains will be the same considering the monomer concentration is constant at the surface; therefore, the same average properties of all polymer chains are produced. The assumptions of the SCM are disagreement with experimental observations because the catalyst particles are porous fragments.

Singh and Merrill (Ref 10) and Galvan and Tirrell (Ref 11, 12) proposed the polymeric flow model (PFM). This model supposes that the catalyst fragments; polymer chains grow form a continuous diffusion of both reagents; and heat takes place through the pseudo-homogeneous polymer matrix. Their supposition represents a big improvement over previous models, although they do not agree with the large number of experimental values as they do not explicitly consider the fragmentation of the catalyst particle and the values of the parameters used by PFM to generate results which are not physically meaningful.

Many papers have been published on models of polymer particle growth and morphology; most of these studies were based on the multigrain model (MGM) of Floyd et al. (Ref 13). In accordance with numerous experiments, the MGM assumes a rapid breakup of the catalyst particles into small fragments, which are distributed throughout the polymer particles. Thus, the large polymer particles (macroparticles) consist of many small molecules (microparticles), which encapsulate these catalyst fragments. For the monomer particles to reach the active sites, they must first be diffused through the pores of macroparticles, between the microparticles, and then to microparticles themselves. In general, the diffusion resistances in both cases are not equal; in addition, they include the possibility of having an equilibrium sorption of monomer particles on the surface of the microparticle. The disadvantage of this model is that it is time consuming when is used the computer to obtain results.

Varshney et al. (Ref 14) used the MGM to describe the simultaneous multicomponent diffusion-cum-reaction taking place in a unifunctional multicomponent catalyst. In this, particles of the more active component are randomly dispersed in a less active near-spherical porous matrix.

The introduction of a mesoparticle scale can be important in the description of mass transfer effects in the heterogeneous polymerization reactor. Debling and Ray (Ref 15) and Kittilsen and Svendsen (Ref 16) demonstrated that a morphological size mesolevel on the order of some tenths of the size of the whole particle exists; the use of traditional MGM that includes mass transfer effects only the macro- and microscales gives conflicting results when the mass transfer resistance at the mesolevel becomes significant.

The MGM was derived for conventional Ziegler-Natta catalysts and only a complete fragmented particle is considered, while a few models specially derived for metallocene catalysts may be found in the literature. Polymerization with a silica-supported metallocene catalyst (Ref 17) shows that, in some cases, fragmentation is a gradual phenomenon.

Bonini et al. (Ref 18) proposed a new particle growth model (PGM). In their model, only the first external shell of the catalyst is supposed to be active in the initial stages of polymerization. The polymer growing in this shell fills the pores of the catalyst, which consequently results in the fragmentation of the shell, and then a layer by layer growth and fragmentation takes place until the whole catalyst is completely fragmented. The final stage is the same as the multigrain structure. The model showed good agreements with the experimental results except for the initial stage of the polymerization. However, their model could not predict large polydispersities.

Alexiadis et al. (Ref 19) derived a more general model from that of Bonini et al. (Ref 18), but with the addition of a further part regarding the unfragmented core for the olefin homopolymerization with metallocene catalysts.

In our previous work, Sultan et al. (Ref 20) developed a single PGM for heterogeneous polymerization of styrene based on MGM; by taking the factor of diffusion at the microparticle level under advisement and the effective diffusion coefficients here is considered to change at any time during particle growth as opposed to MGM. The model has been established to predict the radial monomer concentration within the growing macroparticles, the rate of polymerization and MWD.

The single particle growth of SPS over a silica-supported metollocene catalyst has been observed by Han et al. (Ref 4). The authors noticed that the SPS particle surface was covered with heavily entangled long nanofibrils of 30-50 nm in diameter, which grew out from the active site on the silica particle. The nanofibrils then collapsed and fused on the particle surface as they were exposed to the bulk liquid phase during polymerization. Shear force exerted by agitation in the reactor might have also promoted the adhesion of SPS nanofibrils on the silica particle surface, making them look like a fused layer. As polymerization continued, the buildup of hydraulic forces in the particle porous increased, leading to the fragmentation of the silica support from the particle surface to the interior. Thus, new active centers were exposed by fragmentation and the polymerization rate increased as shown in Fig. 1.

In the present work, a comprehensive model for single particle styrene polymerization is mainly extended from our previous work Sultan et al. (Ref 20) with two main differences. Firstly, this model introduces the mesoparticle scale as a third level in the description of single particle growth by accounting for the monomer diffusion phenomena at three levels, namely, taking the effect of monomer diffusion at the macro-, meso-, and microparticle levels into account. Secondly, the model involves a gradual fragmentation of the catalyst particle for a single particle growth of SPS over a silica-supported metallocene catalyst. In addition, the model combines with the kinetics model to predict the effects of intraparticle mass transfer resistance, initial catalyst particle size, and initial catalyst active site concentration on the polymerization rate, degree of polymerization (DP), and the polydispersity index (PDI) of SPS.

2. Mathematical Model

The time-dependent growth of polymer particles can be expressed as a radial gradient distribution system of monomer concentration, which explains the spatial and temporal physical characteristics of the polymer.

Figure 2 describes the modification of MGM for a single particle growth of the SPS polymer by introducing a mesoparticle scale, in which the catalyst particles cleave to small fragments which are distributed throughout the polymer particles. This means that the large polymer particle (macroparticles) consist of many small polymer particles (meso- and microparticles). The microparticles are assumed to be much

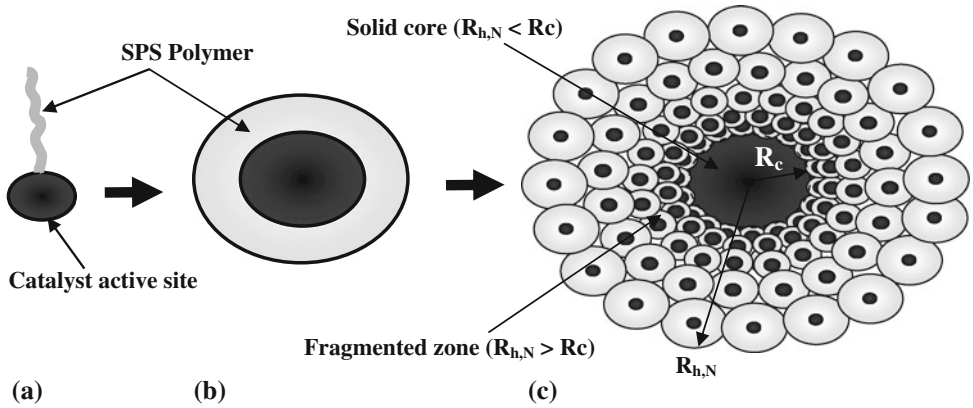

Fig. 1 Schematic representation of the SPS particle growth: (a) Nanofibrils (SPS) polymer grown from the catalyst particle. (b) Nanofibrils SPS polymer collapse and fused on catalyst active site as SCM. (c) Geometry of SPS macroparticles in modified MGM

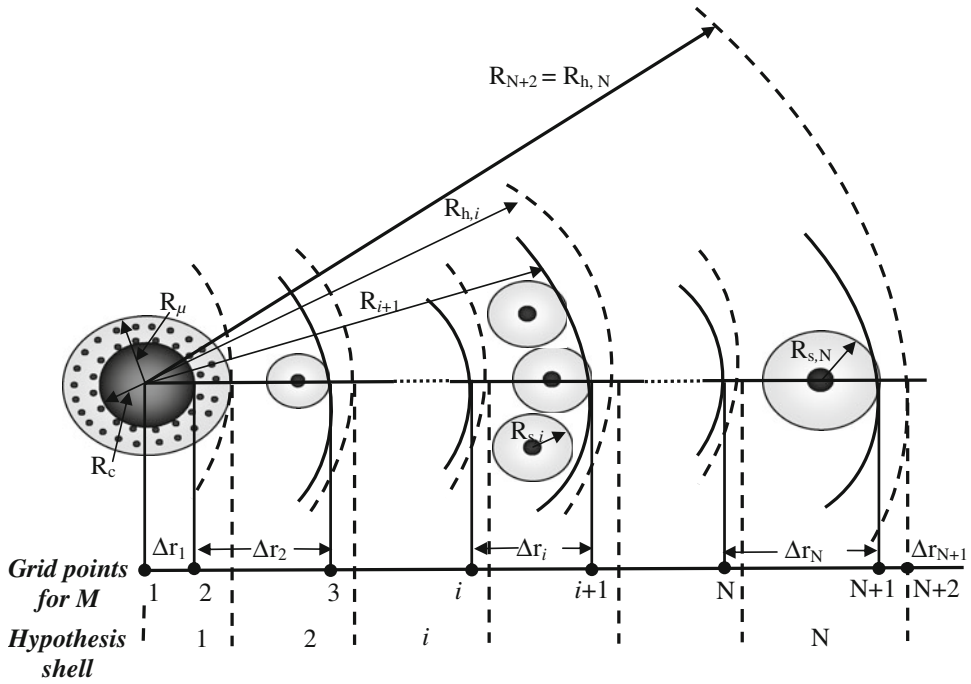

Fig. 2 Schematic representation of modified MGM

smaller than the mesoparticles; thus, the microparticles can be treated as pseudo-homogeneous. Furthermore, one can notice the hypothetical radius of macroparticle shells which can be defined by (Rh_i); whereas, the meso- and microparticle can be placed at the mid-point of each hypothesis shell. At time zero, it is assumed that there is no monomer diffusion toward the catalyst surface which is why the sizes of all shells are equal. Whenever the polymerization starts, all monomer particles diffuse and reach the active site on the catalyst surface. In fact, all the micro- and mesoparticles are surrounded by growing polymer chains. Due to the fact that their size, volume, and position change; it is necessary to update all positions and volumes at any given time interval.

In order to create a PGM, the relation between monomer concentration in the macro-, meso-, and microparticles must be developed.

2.1 Macroparticle Scale Model

The general mass balance for component i in a system with mass transport and reaction is:

$$\frac{dc_i}{dt} + (\nabla \cdot N_i) = -R_{pi} \quad \text{(Eq 1)}$$

where c_i the concentration of component i, N_i is molar flux, and R_{pi} is reaction rate. Consequently, the diffusion equation for a single spherical macroparticle monomer concentration can be as follows:

$$\frac{\partial[M]}{\partial t} = \frac{D_{ef,M}}{r^2}\frac{\partial}{\partial r}\left(r^2\frac{\partial[M]}{\partial r}\right) - R_p \quad \text{(Eq 2)}$$

$$\text{Initial condition at} \quad t = 0, \quad [M] = [M]_o = 0 \quad \text{(Eq 3)}$$

Table 1 Finite difference equation for styrene concentration at *i* position

$$\frac{dM_1}{dt} = \frac{2D_{\mathrm{ef,M},1}(M_2 - M_1)}{(\Delta r_1)^2} - R_{\mathrm{p},1}$$

$$\frac{dM_i}{dt} = \frac{2D_{\mathrm{ef,M},i}}{\Delta r_i + \Delta r_{i-1}}\left[M_{i+1}\left(\frac{1}{\Delta r_i} + \frac{1}{R_i}\right) - M_i\left(\frac{1}{\Delta r_i} + \frac{1}{\Delta r_{i-1}}\right) + M_{i-1}\left(\frac{1}{\Delta r_{i-1}} - \frac{1}{R_i}\right)\right] - R_{\mathrm{p},i}; \quad i = 2, 3, \ldots, N+1$$

$$\frac{dM_{N+2}}{dt} = -M_{N+2}\left[\frac{2k_\mathrm{s}}{\Delta r_{N+1}} + \frac{2D_{\mathrm{ef,M},N+2}}{(\Delta r_{N+1})^2} + \frac{2k_\mathrm{s}}{R_{N+2}}\right] + M_{N+1}\left[\frac{2D_{\mathrm{ef,M},N+2}}{(\Delta r_{N+1})^2}\right] + M_\mathrm{b}\left[\frac{2k_\mathrm{s}}{\Delta r_{N+1}} + \frac{2k_\mathrm{s}}{R_{N+2}}\right] - R_{\mathrm{p},N+2}$$

Boundary condition 1. at $r = 0$, $\dfrac{\partial [M]}{\partial r} = 0$ (Eq 4)

Boundary condition 2. at $r = R_{N+2}$,

$$D_{\mathrm{ef,M}}\frac{\partial [M]}{\partial r} = k_\mathrm{s}([M]_\mathrm{b} - [M]) \quad \text{(Eq 5)}$$

where $[M]$ is the monomer concentration in the macroparticle; $D_{\mathrm{ef,M}}$ is the effective diffusivity of monomer; R_p is the volumetric rate of polymerization in the macroparticle, $[M]_\mathrm{b}$ is the bulk monomer concentration, and k_s is the external film mass transfer coefficient.

Equation (2) is converted to a set of $(N + 2)$ ordinary differential equations (ODEs) of monomer concentration at i position using a finite difference technique that was stated by Finlayson (Ref 21), with regard to the unequally spaced grid points as shown in Fig. 2. These equations are listed in Table 1. In these, subscript i (i = 1, 2, …, $N + 2$), on any variable, indicates its value at the ith grid point. The calculations of (Δr and R) at (ith) position are given in Appendix 1.

The effective diffusion coefficient of a monomer through the polymer macroparticle ($D_{\mathrm{ef,M}}$) was commonly evaluated according to Eq 6, which considers diffusion through a porous medium (Ref 22).

$$D_{\mathrm{ef,M}} = \frac{\varepsilon_\mathrm{M}}{\tau_\mathrm{M}} D_{\mathrm{m,solv}} \quad \text{(Eq 6)}$$

where ε_M and τ_M are the porosity and tortuosity of the macroparticle, respectively. $D_{\mathrm{m,solv}}$ is the diffusivity of monomer in the solvent, which can be appropriately estimated by the Wilke-Chang correlation (Ref 23), according to the following equation:

$$D_{\mathrm{m,solv}} = 7.4 \times 10^{-8}\frac{(\emptyset M_\mathrm{solv})^{0.5} T}{\eta_\mathrm{solv} v_{\mathrm{m,bp}}^{0.6}} \quad \text{(Eq 7)}$$

where M_solv is molecular weight of the solvent, T is the temperature (K), η_solv is the solvent viscosity, and $v_{\mathrm{m,bp}}$ is the molecular volume of the monomer at its boiling point. The interaction between the solvent and the diffusing compound is given by the parameter $\emptyset$, which is equal to unity for nonpolar solvents.

Sarkar and Gupta (Ref 24), enabled the diffusivity to be corrected by a factor proportional to the amount of polymer in the particles, i.e., the term $\varepsilon_\mathrm{M}/\tau_\mathrm{M}$ of Eq 6 for a correction factor equal to the area-fraction of polymer (assumed to be the same as its volume fraction) in the macroparticle at any radial location. Thus, as the particle fills up with polymer, the effective diffusivity decrease as follows:

$$D_{\mathrm{ef,M},1} = D_{\mathrm{ef,M},N+2} = D_{\mathrm{m,solv}} \quad \text{(Eq 8)}$$

$$D_{\mathrm{ef,M},2} = D_{\mathrm{m,solv}} N_1 \frac{R_\mathrm{c}^3}{R_{\mathrm{h},1}^3} \quad \text{(Eq 9)}$$

$$D_{\mathrm{ef,M},i+1} = D_{\mathrm{m,solv}}\frac{(V_{\mathrm{cs},i} - V_{\mathrm{cc},i})}{V_{\mathrm{cs},i}} = D_{\mathrm{m,solv}}\frac{R_{\mathrm{h},i}^3 - R_{\mathrm{h},i-1}^3 - N_i R_\mathrm{c}^3}{R_{\mathrm{h},i}^3 - R_{\mathrm{h},i-1}^3} \quad \text{(Eq 10)}$$

where $V_{\mathrm{cs},i}$ and $V_{\mathrm{cc},i}$ are the volume of the ith shell and the catalyst volume in shell i, respectively, N_i is the number of mesoparticles in ith shell at a given macroparticle radius which can be calculated using porosity ε which has been taken to be a constant, associated with close packed sphere.

$$N_1 = 1 \quad \text{(Eq 11)}$$

$$N_i = 24(1 - \varepsilon)(i - 1)^2; \quad i = 2, 3, \ldots, N \quad \text{(Eq 12)}$$

The volumetric rate of monomer consumption at any radial location, R_p, can be calculated by:

$$R_{\mathrm{p},1} = R_{\mathrm{p},N+2} = 0 \quad \text{(Eq 13)}$$

$$R_{\mathrm{p},2} = \frac{k_\mathrm{p}[C^*][M]_{\mathrm{c},1} N_1 R_\mathrm{c}^3}{R_{\mathrm{h},1}^3}; \quad i = 2, 3, \ldots, N+1 \quad \text{(Eq 14)}$$

$$R_{\mathrm{p,i}} = \frac{k_\mathrm{p}[C^*][M]_{\mathrm{c},i-1} N_{i-1} R_\mathrm{c}^3}{\left(R_{\mathrm{h,i}}^3 - R_{\mathrm{h,i-1}}^3\right)}; \quad i = 2, 3, \ldots, N+1 \quad \text{(Eq 15)}$$

The corresponding overall time-dependent polymerization rate can be estimated as follows:

$$R_{\mathrm{p,overall}} = \frac{(\mathrm{mw})_\mathrm{sty} k_\mathrm{p}[C^*]\sum_{i=1}^{N}(N_i[M]_{\mathrm{c},i})}{\rho_\mathrm{c}\sum_{i=1}^{N} N_i} \quad \left(\frac{\mathrm{g\ SPS}}{\mathrm{g\ cat\ h}}\right) \quad \text{(Eq 16)}$$

where $M_{\mathrm{c,i}}$ is the monomer concentration at the catalyst surface at any radial position, as illustrated in section 2.3.

For a single spherical particle, moving in a continuous liquid phase with a relative velocity u, the external film mass transfer coefficients (k_s) can be calculated by the well-known Ranz-Marshall correlations (Ref 25).

$$Sh = \frac{k_\mathrm{s} d_\mathrm{p}}{D} = 2 + 0.6 Sc^{0.33} Re^{0.5} \quad \text{(Eq 17)}$$

$$\text{where } Sc = \frac{\mu}{\rho D} \text{ is the Schmidt number and } Re = \frac{\rho u d_\mathrm{p}}{\mu} \text{ is the Reynolds number} \quad \text{(Eq 18)}$$

2.2 Mesoparticle Scale Model

In this section, the relationship between the mesoparticle monomer concentration $[M]_\mathrm{s}$ and the macroparticle monomer concentration $[M]$ has been developed. The mesoparticles are assumed to be of spherical shape and with a catalyst evenly

distributed inside. The diffusion equation for a single spherical mesoparticle monomer is as follows:

$$\frac{\partial [M]_s(r,t)}{\partial t} = \frac{D_{ef,s}}{r^2}\frac{\partial}{\partial r}\left(r^2\frac{\partial [M]_s}{\partial r}\right) - R_P \quad \text{(Eq 19)}$$

where $M_s(r, t)$ is the monomer concentration in the mesoparticle and $D_{ef,s}$ is the effective diffusivity across the mesoparticle. The initial and boundary conditions are given by:

$$\text{Initial condition} \quad \text{at } t = 0, \quad [M]_s = [M]_{so} = 0 \quad \text{(Eq 20)}$$

$$\text{Boundary condition 1.} \quad \text{at } r = 0, \quad \frac{\partial [M]_s}{\partial r} = 0 \quad \text{(Eq 21)}$$

$$\text{Boundary condition 2.} \quad \text{at } r = R_s, \quad [M]_s = [M]_s^* = k_{e,s}[M] \le [M] \quad \text{(Eq 22)}$$

where R_s is the radius of the mesoparticles, $[M]_s^*$ is the equilibrium concentration of monomer in the interface between the meso- and macroparticles and $k_{e,s}$ represents the corresponding equilibrium constant for monomer absorption in the mesoparticle. All these variables generally depend on their position in the macroparticle. If one solves the diffusion reaction equation for this ideal system, using the quasi steady state approximation (QSSA), it is possible to calculate a volume-averaged monomer concentration in the particle, and thus the effective reaction rate as Thiele did (Ref 26). In this way we can link the monomer concentration in the macropore $[M]$ outside a mesoparticle at the ith shells with the average concentration inside the mesoparticle, $[M]_s$ which can be put as stated below:

$$[M]_{s,i} = \frac{3}{\alpha_{s,i}^2}\left(\alpha_{s,i}\coth\alpha_{s,i} - 1\right)[M_i] \quad \text{(Eq 23)}$$

where α_s is a Thiele modulus $\alpha_{s,i} = R_{s,i}\sqrt{k_p C^*/D_{ef,s}}$. From Eq 23, a significant monomer concentration difference may exist between the meso- and macroparticle, depending on the Thiele modulus α_s. The mesoparticle diffusion effectiveness factor (η_s) may be defined as:

$$[M]_s = \eta_s[M] \quad \text{(Eq 24)}$$

$$\text{where} \quad \eta_s = \frac{3}{\alpha_s^2}(\alpha_s\coth\alpha_s - 1) \quad \text{(Eq 25)}$$

Monomer diffusion in the mesoparticles will in general not only bring the monomer to the active sites within the mesoparticles, but also contribute to the total radial transport in the macroparticle. When calculating this contribution to the macroparticle mass transport, the effective diffusivity in the mesoparticles ($D_{ef,s}$) has to be adjusted for the mesoparticle fraction of the total area. In a cross section of the particle, there will be a given area of macropores and a given area of mesoparticles. The area of macropores is already included through the macroparticle porosity ε_M in the effective macroparticle diffusivity. However, the $D_{ef,s}$ based on the total particle volume must be corrected for the mesoparticles volume fraction, corresponding to $(1 - \varepsilon_M)$, and then be evaluated according to Eq 26.

$$D_{ef,s} = \frac{\varepsilon_s(1-\varepsilon_M)}{\tau_s}D_{m,solv} \quad \text{(Eq 26)}$$

where ε_s and τ_s are the porosity and tortuosity of the mesoparticle, respectively.

2.3 Microparticle Scale Model

The monomer concentration profile in the spherical microparticle is the same as that in the SCM model.

$$\frac{\partial [M]_\mu(r,t)}{\partial t} = \frac{D_{ef,\mu}}{r^2}\frac{\partial}{\partial r}\left(r^2\frac{\partial [M]_\mu}{\partial r}\right) \quad \text{(Eq 27)}$$

where $M_\mu(r, t)$ is the monomer concentration in the microparticle and $D_{ef,\mu}$ is the effective diffusivity. In the microparticles, all of the active sites are assumed to be at the catalyst core at $r = R_c$. Thus, the initial and boundary conditions are given by:

$$\text{Initial condition} \quad \text{at } t = 0, \quad [M]_\mu = [M]_{\mu o} = 0 \quad \text{(Eq 28)}$$

$$\text{Boundary condition 1.} \quad \text{at } r = R_c, \quad 4\pi R_c^2 D_{e,\mu}\frac{\partial [M]_\mu}{\partial r} = \frac{4}{3}\pi R_c^3 R_{pc} \quad \text{(Eq 29)}$$

$$\text{Boundary condition 2.} \quad \text{at } r = R_\mu, \quad [M]_\mu = [M]_\mu^* = k_{e,\mu}[M]_s \le [M]_s \quad \text{(Eq 30)}$$

where R_c is the catalyst particle radius, R_μ is the microparticle radius and $[M]_\mu^*$ is the equilibrium concentration of monomer in the interface between micro- and mesoparticles, $k_{e,\mu}$ represents the corresponding equilibrium constant for monomer absorption in the microparticle.

Assuming effective diffusivity ($D_{ef,\mu}$) is constant across the microparticle and employs the QSSA, which is valid since the microparticle diffusion times are very short, Eq 27 is integrated to give monomer concentration profiles across the microparticles.

$$[M]_\mu = k_{e,\mu}[M]_s + \frac{R_c^3 k_p[C^*][M]_c}{3D_{e,\mu}}\left(\frac{1}{R_\mu} - \frac{1}{r}\right) \quad \text{(Eq 31)}$$

The monomer concentration at the surface of catalyst fragment ($r = R_c$) is then.

$$[M]_c = \frac{k_{e,\mu}[M]_s}{1 + \frac{1}{3}\frac{\alpha_\mu^2(\emptyset_\mu - 1)}{\emptyset_\mu}} \quad \text{(Eq 32)}$$

where α_μ is a Thiele modulus, $\alpha_\mu = R_c\sqrt{k_p C^*/D_{ef,\mu}}$ and $\emptyset_\mu = R_\mu/R_c$ is the microparticle growth factor.

Equation 32 shows that a significant concentration gradient may exist between the surface of the mesoparticle and the catalyst surface, depending on the particle growth factor $\emptyset_\mu$ and the Thiele modulus α_μ. The microparticle diffusion effectiveness factor may be defined as:

$$[M]_c = \eta_\mu[M]_s \quad \text{(Eq 33)}$$

$$\text{where} \quad \eta_\mu = \frac{1}{1 + \frac{1}{3}\frac{\alpha_\mu^2(\emptyset_\mu - 1)}{\emptyset_\mu}} \quad \text{(Eq 34)}$$

Using both the effectiveness factors at the mesoparticle (Eq 24) and microparticle level (Eq 33), the overall polymerization rate per volume of particle, Eq 16 can be written as:

$$R_{p,overall} = \frac{(mw)_{sty}k_p[C^*]\sum_{i=1}^{N}\left(N_i\eta_{\mu,i}\eta_{s,i}[M]_i\right)}{\rho_c\sum_{i=1}^{N}N_i} \quad \text{(Eq 35)}$$

Table 2 Kinetic mechanism of styrene polymerization over metallocene catalyst

Description	Reaction
Catalyst activation	$C_o + \text{MAO} \xrightarrow{ka} C^*$
Propagation	$C^* + M_c \xrightarrow{kp} L_1$
Chain transfer to monomer	$L_n + M_c \xrightarrow[ktM]{kp} L_{n+1}$ $L_n + M_c \longrightarrow D_n + L_1$
β-hydrogen elimination	$L_n \xrightarrow{kt\beta} D_n + C^*$
Catalyst deactivation	$C^* \xrightarrow{kd} D^* l$
	$L_n \xrightarrow{kd} D^* l$

Table 3 Rate and moment equations of styrene polymerization over metallocene catalyst

$$\frac{d[C^*]}{dt} = -k_d[C^*] - k_p[C^*][M]_c + k_{t\beta}\lambda_{Lo}$$
$$\frac{d[M]_c}{dt} = -k_p[L][M]_c - k_{tM}[L][M] \approx -k_p[L][M]_c$$
$$\frac{d\lambda_{Lo}}{dt} = k_p[C^*][M]_c - k_{t\beta}\lambda_{Lo} - k_d\lambda_{Lo}$$
$$\frac{d\lambda_{L1}}{dt} = k_p[C^*][M]_c + k_p\lambda_{Lo}[M]_c + k_{tM}[M]_c(\lambda_{Lo} - \lambda_{L1}) - k_{t\beta}\lambda_{L1} - k_d\lambda_{L1}$$
$$\frac{d\lambda_{L2}}{dt} = k_p[C^*][M]_c + k_p[M]_c(2\lambda_{L1} + \lambda_{Lo}) + k_{tM}[M]_c(\lambda_{Lo} - \lambda_{L2}) - k_{t\beta}\lambda_{L2} - k_d\lambda_{L2}$$
$$\frac{d\lambda_{Do}}{dt} = k_{t\beta}\lambda_{Lo} + k_d\lambda_{Lo} + k_{tM}\lambda_{Lo}[M]_c$$
$$\frac{d\lambda_{D1}}{dt} = k_{t\beta}\lambda_{L1} + k_d\lambda_{L1} + k_{tM}\lambda_{L1}[M]_c$$
$$\frac{d\lambda_{D2}}{dt} = k_{t\beta}\lambda_{L2} + k_d\lambda_{L2} + k_{tM}\lambda_{L2}[M]_c$$

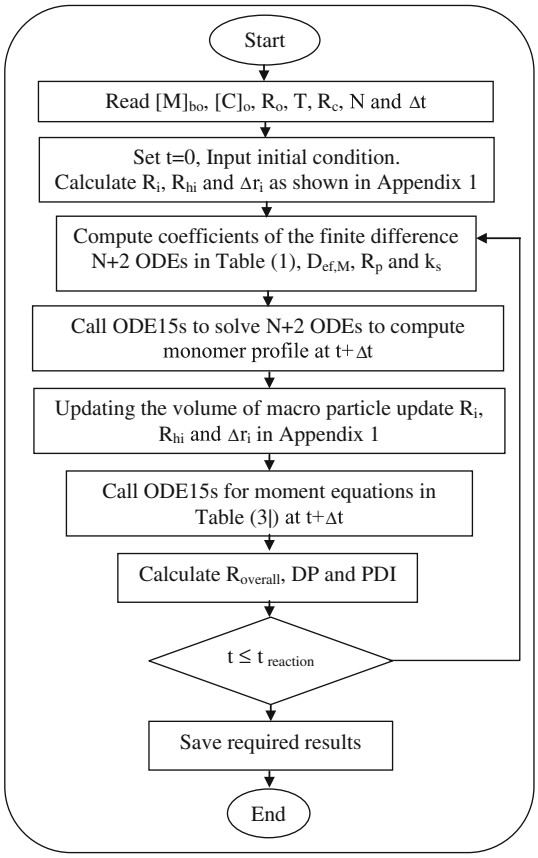

Scheme 1 Algorithm of computer simulation program

Although the site deactivation mechanisms and kinetics are not well understood for most of the transition metal catalyzed polymerization processes, first-order deactivation kinetics have been generally well accepted. If we assume first-order deactivation kinetics, the polymerization rate equation can be expressed as follows:

$$R_{p,\text{overall}} = \frac{(\text{mw})_{sty} k_p [C^*]_o \exp(-k_d t) \sum_{i=1}^{N} (N_i \eta_{\mu,i} \eta_{s,i} [M]_i)}{\rho_c \sum_{i=1}^{N} N_i} \left(\frac{\text{g SPS}}{\text{g cat h}}\right) \quad \text{(Eq 36)}$$

where k_p and is the constant propagation rate and k_d is the catalyst active sites concentration, which can be calculated from the kinetic reaction scheme of styrene polymerization as shown in Table 2.

Finally, the calculation of polymer properties was carried out by means of the well-known moment technique (Ref 27). The MWD was evaluated by calculating its leading moments, both for living and dead polymer. The nth moment of the chain length distribution of growing polymer is given by a weighted sum of polymer concentrations defined as:

$$\lambda_{Lk} = \sum_{n=1}^{\infty} n^k [L_n] \quad \text{(Eq 37)}$$

$$\lambda_{Dk} = \sum_{n=1}^{\infty} n^k [D_n] \quad \text{(Eq 38)}$$

where λ_{Lo} represents the total concentration of live polymer and D_n denotes the total dead polymer concentration. The rate and moment equation of styrene polymerization are derived as shown in Table 3.

The M_n and M_w of the polymer are obtained by multiplying theses chain lengths with the molecular weight of unit styrene monomer $(\text{mw})_{sty}$ using the following equations:

$$M_n = \left[\frac{\lambda_{L1} + \lambda_{D1}}{\lambda_{Lo} + \lambda_{Do}}\right] (\text{mw})_{sty} \quad \text{(Eq 39)}$$

Table 4 Reference values of parameters for simulation

Parameter	Value	Unit
$[M]_{bo}$	1.98	mol/L
$[C]_o$	1.55×10^{-4}-3.11×10^{-4}	mol/L
R_o	20-50	μm
R_M	100	μm
R_s	$0.3R_M$	μm
R_c	0.2-0.5	μm
ε_M	0.4	…
ε_s	0.03	…
τ_M	2.0	…
τ_s	3.0	…
$D_{ef,\mu}$	1×10^{-12}	m^2/s
T_o	323-343	K
k_p	$k_p = 4.95 \times 10^{29} \exp\left(\frac{-169{,}000}{R_{gas}T}\right)$	L/(mol h)
k_d	$k_d = 6.2 \times 10^{18} \exp\left(\frac{-122{,}400}{R_{gas}T}\right)$	h^{-1}
k_t	$k_{t\beta} = 3.2 \times 10^{20} \exp\left(\frac{-128{,}800}{R_{gas}T}\right)$	h^{-1}
k_{tM}	$k_{tM} = 4.8 \times 10^{19} \exp\left(\frac{-125{,}990}{R_{gas}T}\right)$	L/(mol h)
η_{solv}	$\ln \eta_{solv} = 11.64 + \frac{1.006 \times 10^4}{T}$	cp

Table 5 Reaction conditions and experimental data of SPS polymerization

Run	$[M]_{bo}$, mol/L	R_o, μm	$[C^*]_o \times 10^4$, mol Ti/L	T, K	Time, min	Yield, g	Polymerization rate, g SPS/(g cat h)	DP × 10^{-3}	PDI
1-1	1.98	20	3.11	343	10	7.8	468.0	0.73	3.0
1-2					20	11.2	336.0	…	…
1-3					30	13.5	270.0	0.75	3.16
1-4					60	15.2	152.0	0.71	2.87
1-5					120	16.8	84.0	0.69	2.8
2-1		50	3.11	343	10	2.41	289.2	0.54	3.8
2-2					20	7.8	234.0	…	…
2-3					30	10.77	215.4	0.57	3.5
2-4					60	13.33	133.3	0.54	3.67
2-5					120	15.6	78.0	0.52	3.3
3-1		20	1.55	343	10	2.5	300.0	1.15	2.2
3-2					20	4.5	270.0	…	…
3-3					30	5	200.0	1.14	2.3
3-4					60	6.5	130.0	1.14	2.3
3-5					120	4.0	40.0	1.17	2.2
4-1					10	3.59	215.46	0.49	4.0
4-2					20	6.33	190.0	…	…
4-3		20	3.11	323	30	9.22	184.68	0.44	4.0
4-4					60	9.64	96.44	0.44	4.0
4-5					120	2.1	10.26	0.47	3.9

Polymerization condition: 100 mL of styrene and *n*-heptane were used (25 vol.% styrene), [Al]/[Ti] = 300

$$M_w = \left[\frac{\lambda_{L2} + \lambda_{D2}}{\lambda_{L1} + \lambda_{D1}}\right](mw)_{sty} \quad \text{(Eq 40)}$$

The DP and PDI is given by:

$$DP = \frac{M_n}{(mw)_{sty}} = \frac{(\lambda_{L1} + \lambda_{D1})}{(\lambda_{Lo} + \lambda_{Do})} \quad \text{(Eq 41)}$$

$$PDI = \frac{M_w}{M_n} = \frac{(\lambda_{L2} + \lambda_{D2})(\lambda_{Lo} + \lambda_{Do})}{(\lambda_{L1} + \lambda_{D1})^2} \quad \text{(Eq 42)}$$

3. Solution Methodology

In the present work, the modified MGM, i.e., equations in Table 1 are solved simultaneously with the kinetics model, i.e., equations in Table 3 to obtain the polymerization rate, DP and PDI under intraparticle mass transfer limitations and catalyst properties (initial catalyst active site concentration and initial catalyst size). In Scheme 1, the details of the computer simulation program algorithm are presented with all the related equations that are used in this model.

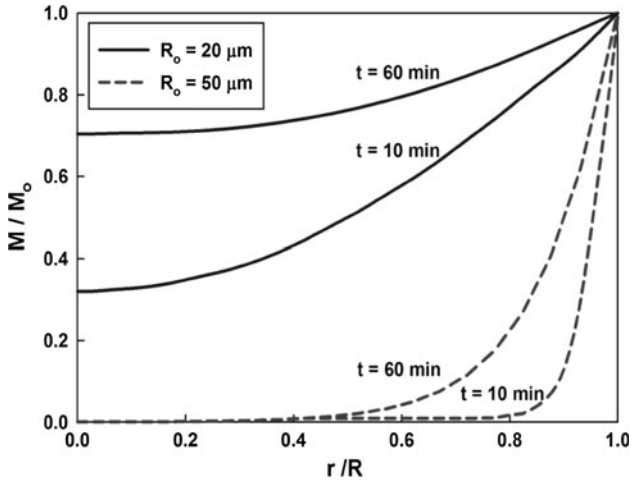

Fig. 3 Effect of initial catalyst particle size on the spatial styrene concentration in the polymer particle at two different polymerization time ($[M]_o$ = 1.98 mol/L, $[C^*]_o = 3.11 \times 10^{-4}$ mol/L, T = 70 °C)

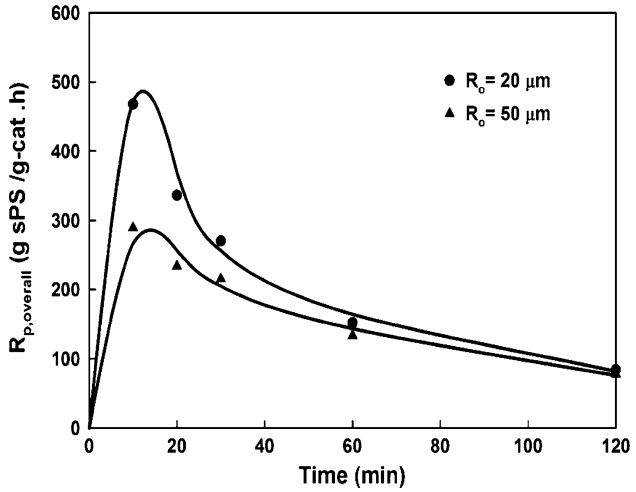

Fig. 4 Effect of initial catalyst particle size on the overall polymerization rate (symbols—experimental data, lines—model) ($[M]_o$ = 1.98 mol/L, $[C^*]_o = 3.11 \times 10^{-4}$ mol/L, T = 70 °C)

The model was implemented by using the Matlab M-Function program and was solved with a subroutine called ODE15s, which is usually used with stiff differential equations. The set of realistic parameter values included the physical and transport properties of the reaction mixture and the kinetic rate constants. These parameters were selected and are listed in Table 4.

4. Experimental Work

4.1 Materials

Styrene (Aldrich) was vacuum distilled over calcium hydride and activated alumina was used to remove inhibitor from the monomer. *n*-Heptane (Fisher Scientific) was used as a diluents and it was purified by being refluxed over sodium and benzophenone in nitrogen atmosphere. $CpTiCl_3$ (cyclopentadienyltitaniumtrichloride) (Aldrich) and methylaluminoxane (MAO, Aldrich) were used as-supplied without further purification. Silica gel (Davisil 633, Aldrich, average pore size: 6 nm) was used as a catalyst support.

4.2 Preparation of Supported Catalysts

Silica gel was calcined at 300 °C for 24 h. The calcined silica gel was then treated with an MAO solution (2.3 mmol of MAO and 30 mL of toluene per 3 g of silica gel, mixed at 50 °C for 1.5 h), washed with toluene, and dried. Then, the silica support was mixed with a $CpTiCl_3$ catalyst solution (1.5 mmol of $CpTiCl_3$ and 55 mL of toluene per 3 g of MAO silica, mixed at 50 °C for 1 h), washed with toluene, and dried for 24 h. The Al and Ti loadings measured by inductively coupled plasma emission spectroscopy (ICP) were 1.31×10^{-3} mol Al/g catalyst and 2.74×10^{-4} mol Ti/g catalyst, respectively.

4.3 Polymerization Reaction

Styrene polymerization experiments were carried out using a 250 mL reactor equipped with a stainless steel agitator under nitrogen atmosphere. Predetermined amounts of monomer, solvent, catalyst, and MAO were charged into the reactor. The agitator speed was maintained constant during polymerization. After polymerization, the reaction mixture was removed from the reactor, washed with an excess amount of acidified methanol 10 vol.% of hydrochloric acid, and dried. Since the reactor had no provisions for sampling during the polymerization, the polymer yield versus time profiles were obtained by conducting the individual experiments under the same reaction conditions but terminated at different reaction times. The polymerization rate values were determined by numerically differentiating a polymer yield versus time curve. The methyl ethyl ketone (MEK) insoluble fraction was used as a quick but approximate measure of syndiotacticity. Most of the SPS samples showed that the MEK insoluble fractions were in the range of 92-94%. The feed catalyst particle size was determined based on diffraction of a light source by the samples under analysis using a particle size analyzer (laser diffraction analyzer, CILAS 1180 Liquid). The number and weight average molecular weight were determined by gel permeation chromatography (GPC) with 1,2,3-trichlorobenzene using PLgel® 10 μm MIXED-B column.

5. Results and Discussion

Styrene polymerization experiments were carried out with a different initial catalyst particle size (R_o), an initial catalyst active site concentration ($[C^*]_o$), and a different bulk phase polymerization temperature (T). The same batch of catalyst was used in all these experiments to minimize the run-to-run variations in catalyst activity. Table 5 shows a summary of experimental results for 20 polymerization runs, whereby the same amount of catalyst and Al/Ti mole ratio was used in every experiment.

5.1 Effects of Initial Catalyst Particle Size (R_o)

In slurry polymerization, mass transfer effects in polymer particles are frequently significant, especially in the early

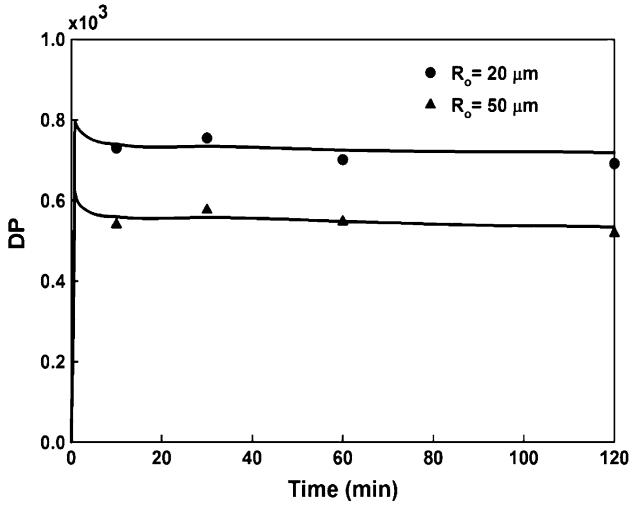

Fig. 5 Effect of initial catalyst particle size on the degree of polymerization (DP) (symbols—experimental data, lines—model) ($[M]_o$ = 1.98 mol/L, $[C^*]_o = 3.11 \times 10^{-4}$ mol/L, T = 70 °C)

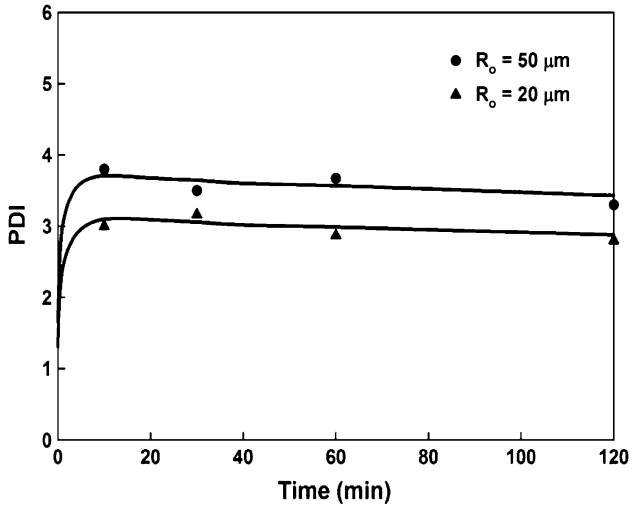

Fig. 6 Effect of initial catalyst particle size on the polydispersity index (PDI) (symbols—experimental data, lines—model) ($[M]_o$ = 1.98 mol/L, $[C^*]_o = 3.11 \times 10^{-4}$ mol/L, T = 70 °C)

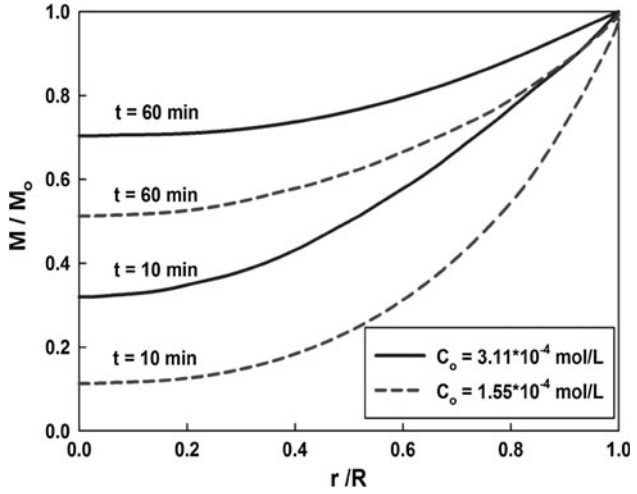

Fig. 7 Effect of initial catalyst concentration on the spatial styrene concentration in the polymer particle at two different polymerization time ($[M]_o$ = 1.98 mol/L, R_o = 20 μm, T = 70 °C)

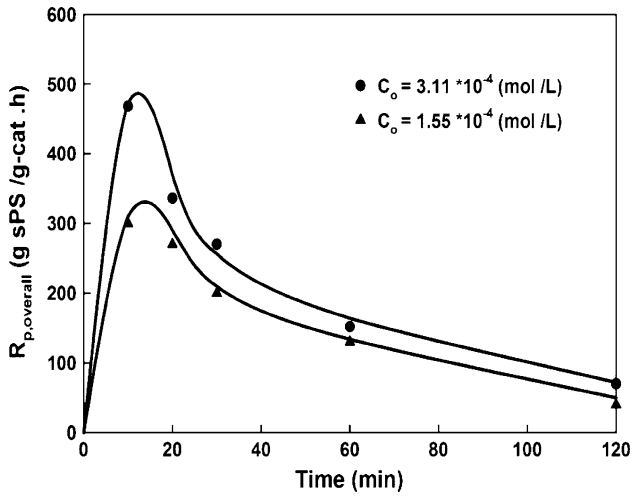

Fig. 8 Effect of initial catalyst concentration on the overall rate of polymerization (symbols—experimental data, lines—model) ($[M]_o$ = 1.98 mol/L, R_o = 20 μm, T = 70 °C)

stages of polymerization. This comes about because in the initial stages of polymerization, the volumetric rate of reaction is at a maximum and the surface area exposed to monomer source (the bulk liquid phase) is at a minimum. Moreover, the effects of intraparticle mass transfer will be most pronounced for large catalyst particles and high catalyst activities, besides the intraparticle mass transfer resistance in the pores of the growing polymer particles. While the former will decrease with time as the volumetric reaction rate decreases, the latter will increase slightly with time as the polymer film surrounding the active sites becomes thicker, and as a result, significant mass limitations can be experienced. This is better shown in Fig. 3 in which the styrene concentration is plotted with respect to radial position for two initial catalyst sizes (R_o) at different polymerization times. As can be seen, when large catalyst particles are employed, significant mass transfer limitations can arise within the growing polymer particle.

Figure 4 depicts the effect of initial catalyst particle size (R_o) on the overall polymerization rate. It can be seen that increasing the size of the catalyst particles leads to a decrease in the polymerization rate. As the initial catalyst particle size increases intraparticular diffusional limitation increases, which is reflected by a decrease in the interfacial contribution to the total polymer formation decreases (due to a decrease in the solid-liquid interfacial area), resulting in a lowering of the polymerization rate.

One of the biggest secrets in polymerization using a catalyst is the increase in the PDI that is generally observed. According to the hypothesis, and with respect to the existence of mass transfer resistance and the effect of initial catalyst particle size, a variation was observed in the concentration of monomer particles on the surface of the catalyst particles. However, such a variation in the concentration is higher in the outer regions than in the interior regions of these particles. As a result, the polymer produced has different molecular weights; a state that

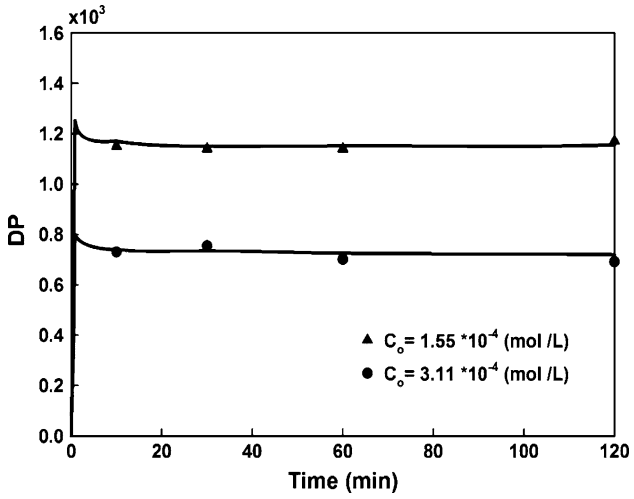

Fig. 9 Effect of initial catalyst concentration on the degree of polymerization (DP) (symbols—experimental data, lines—model) ($[M]_o$ = 1.98 mol/L, R_o = 20 μm, T = 70 °C)

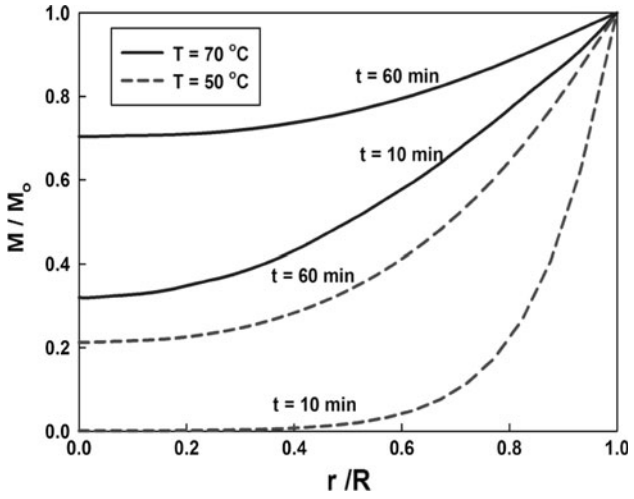

Fig. 11 Effect of bulk phase temperature on the spatial styrene concentration at two different polymerization time ($[M]_o$ = 1.98 mol/L, $[C^*]_o = 3.11 \times 10^{-4}$ mol/L, R_o = 20 μm)

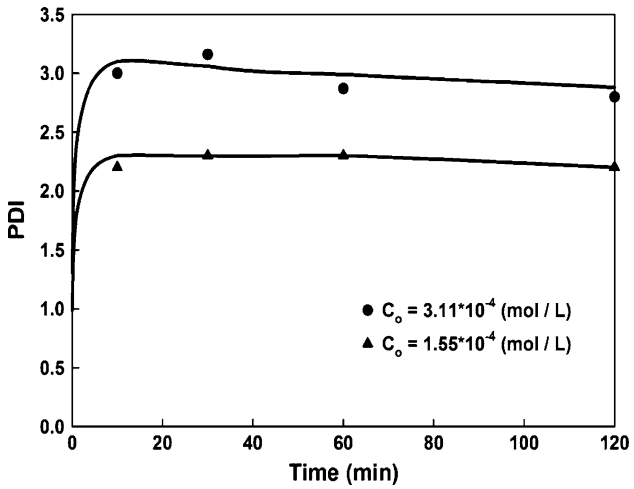

Fig. 10 Effect of initial catalyst concentration on the polydispersity index (PDI) (symbols—experimental data, lines—model) (M_o = 1.98 mol/L, R_o = 20 μm, T = 70 °C)

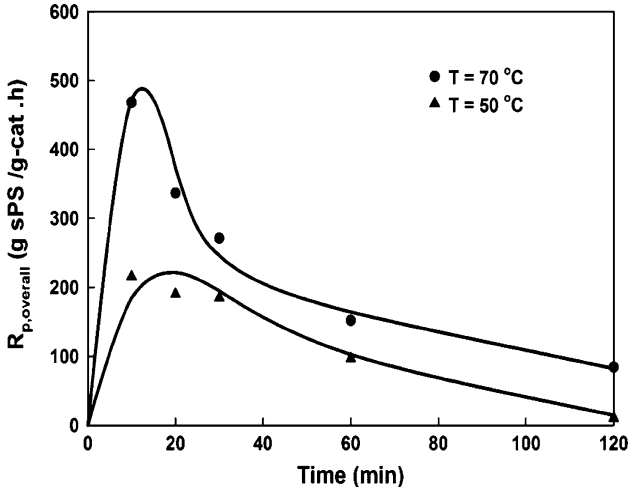

Fig. 12 Effect of bulk phase temperature on the overall polymerization rate (symbols—experimental data, lines—model) ($[M]_o$ = 1.98 mol/L, $[C^*]_o = 3.11 \times 10^{-4}$ mol/L, R_o = 20 μm)

helps gives a large (PDI). In this model and assuming the catalyst particles contain a single active site, a large (PDI) was observed in the first minutes of polymerization at different mass transfer resistance and initial catalyst size.

The effect of initial catalyst particle size on the DP and PDI is shown in Fig. 5 and 6, respectively. From these figures it can be observed that the DP increases while the PDI of the polymer decreases when the R_o is lowered from 50 to 20 μm under the condition that all other values are equal. The reason why the DP is higher for a lower R_o value is because of lower diffusion resistances encountered in small catalyst particles which make the difference of monomer concentration between the inside and outside of the particle fade. So with single site catalysts, the larger initial catalyst particles can give rise to high PDI.

5.2 Effects of Initial Catalyst Concentration ($[C^*]_o$)

The effect of the initial catalyst active site concentration ($[C^*]_o$) at different polymerization times on the radial profile of the styrene concentration is shown in Fig. 7. It demonstrated that at the early step of polymerization, the profile of styrene concentration in the polymer particle is steep, which means that the effect of the mass transfer resistance is significant. Thereafter, the intraparticle mass transfer resistance decreases as a result of a low styrene consumption rate due to catalyst deactivation after a longer polymerization time.

Figure 8 shows the effect of initial catalyst active site concentration on the polymerization rate. It can be observed that the rate of polymerization decreases when $[C^*]_o$ is lowered from 3.11×10^{-4} to 1.55×10^{-4} mol/L. Lowering $[C^*]_o$ leads to two opposite effects: a kinetic effect, i.e., a decrease in the rate of polymerization due to a lowering of $[C^*]_o$ itself in the (k_p $[C^*]$ $[M]_i$) term, and a diffusional resistance leading to a higher monomer concentration value inside the macroparticle. Obviously, the former effect predominates as far as the rate of polymerization is concerned. Higher monomer concentrations inside the macroparticle lead to a higher local DP value as shown in Fig. 9, since the

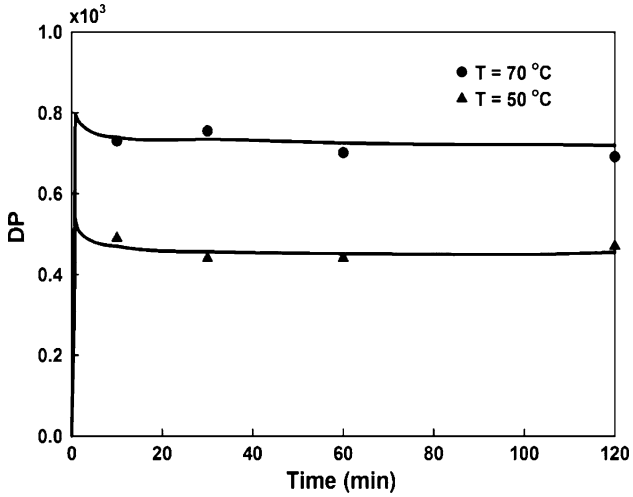

Fig. 13 Effect of bulk phase temperature on the degree of polymerization (DP), (symbols—experimental data, lines—model) ($[M]_o$ = 1.98 mol/L, $[C^*]_o = 3.11 \times 10^{-4}$ mol/L, R_o = 20 μm)

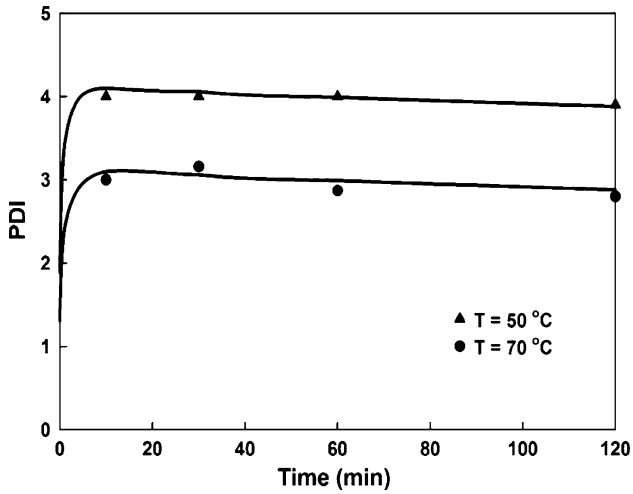

Fig. 14 Effect of bulk phase temperature on the polydispersity index (PDI), (symbols—experimental data, lines—model), ($[M]_o$ = 1.98 mol/L, $[C^*]_o = 3.11 \times 10^{-4}$ mol/L, R_o = 20 μm)

rate of propagation ($k_p\,[C^*]\,[M]_i$) has gone up relative to the rate of chain termination, thus leading to lower (PDI) as shown in Fig. 10.

5.3 Effects of Bulk Phase Temperatures (T)

The evolutions of styrene concentration are plotted with respect to radial position at two reaction times for two different bulk phase temperature as shown in Fig. 11. It is apparent that serious internal mass transfer limitations can arise early in the polymerization process for low temperature values. This means that the local particle polymerization rate will vary with the radial position. On the other hand, for temperature larger values (e.g., $T > 70$ °C), the local polymerization rate will be independent of the radial position almost from the start of polymerization. This means that increased local particle polymerization rates can be obtained, which can lead to excessive particle overheating.

Figure 12 shows the polymerization rate curves at different bulk phase temperature. From this figure, it can be clearly seen that the polymerization rate increase as the temperature rises because the polymerization rates are exponentially temperature dependent functions according to Arrhenius' law. Therefor the polymerization rate increases and the catalyst deactivation changes quicker as the temperature increases.

The effect of bulk phase temperature on the DP is shown in Fig. 13. From this figure, it is revealed that a uniform increase in the DP of the polymer was obtained by increasing the bulk phase temperature, because the deactivation of catalyst leads to an increase in the concentration of monomer in the particle. This in turn leads to an increase in the molecular weight with the passage of time.

Figure 14 depicts the effect of bulk phase temperature on the PDI. It has been noticed that the PDI value decreases with an increase in the polymerization temperature, because the increasing the propagation rate relative to the rate of chain termination leads to lower PDI.

6. Conclusion

A detailed mathematical model for single particle growth of styrene polymerization over a silica-supported metallocene catalyst has been presented. The model was derived based on the modification of the well-known MGM by introducing the mesoparticle scale as a third level in the description of the particle morphology; The mesolevel, with a length scale between the size of the microparticles and the size of the whole particle. The polymer particles can be regarded as being composed of agglomerates of mesoparticles, with a size of some tenths of the size of the whole particle. The model presented here can account for a variable monomer concentration around these mesoparticles and can estimate the influence these have on the total mass transfer in the particles.

The model shows that given typical parameters, the main path for mass transport in the particles is a radial diffusion in the macropores followed by diffusion in a tangential direction to the active sites at the mesoparticle level. The mesoscale level contributes only to a small fraction of the total radial mass transport.

As a rule of thumb, the introduction of the mesolevel in single particle models should be considered when the macroscale diffusion resistance becomes important and the mesolength scale is about 30% of the macrolength scale. For more severe macroscale diffusion resistance, even smaller mesoparticles can induce significant effects.

In addition, the model combines with the kinetics model to predict the effects of intraparticle mass transfer resistance, initial catalyst particle size, and initial catalyst active site concentration on the polymerization rate, DP, and the PDI of SPS. It can be concluded from the model simulation results that, the degree of diffusion resistance is dependent on the physical properties of the catalyst and the effects of the polymerization rate are stronger than those of the polymer properties.

Moreover, the validation of the model with the experimental data agree well with the results and shows that the model is able to predict a correct monomer concentration profile in each macro-, meso-, and microparticle, polymerization rate, particle growth factor and the most important polymer properties represented by DP and PDI.

Acknowledgments

The authors would like to thank University Sains Malaysia (USM) for funding this project under Research University Scheme

No. (1001/PJKIMIA/811107). The first author gratefully acknowledges the USM for supporting this work under USM Fellowship.

Appendix

The changes in the shells volume, (ΔV_i) and the location of the grid points (R_i) with time are given in this section. As shown in Fig. 2. The hypothetical shell can be defined as ($R_{h,i-1} \le r \le R_{h,i}$) such that the entire polymer produced (since time $t = 0$) by the catalyst particles of radius (R_c) are accommodated in it. In the interval (t to $t + \Delta t$), the volume of microparticles ($V_{\mu,i}$) in the first shell are given by:

$$\frac{dV_{\mu,i}}{dt} = \frac{k_p C^* M_{\mu,i}\left(\frac{4\pi}{3}R_c^3\right)(\mathrm{MW})}{\rho_p}; \quad i = 1,2,\ldots,N \qquad \text{(Eq 1.1)}$$

With $V_{\mu,i}$ ($t = 0$) being the initial volume of microparticle in the first shell.

$$V_{\mu,i}(t=0) = \frac{4\pi}{3}R_c^3 \qquad \text{(Eq 1.2)}$$

The total volume of polymer (V_i), the volume of mesoparticle ($V_{s,i}$) produced at ith shell are given by:

$$\frac{dV_i}{dt} = \frac{k_p C^* M_{s,i}\left(N_i\frac{4\pi}{3}R_c^3\right)(\mathrm{MW})}{\rho_p} \quad i = 2,3,\ldots,N \qquad \text{(Eq 1.3)}$$

$$\frac{dV_{s,i}}{dt} = \frac{k_p C^* M_{s,i}\left(\frac{4\pi}{3}R_c^3\right)(\mathrm{MW})}{\rho_p}; \quad i = 2,3,\ldots,N \qquad \text{(Eq 1.4)}$$

With V_i ($t = 0$) and $V_{s,i}$ ($t = 0$) being the initial total volume and volume of every polymer mesoparticle of ith volume, respectively.

$$V_i(t=0) = \frac{N_i\left(\frac{4\pi}{3}R_c^3\right)}{(1-\varepsilon)}; \quad i = 2,3,\ldots,N \qquad \text{(Eq 1.5)}$$

$$V_{s,i}(t=0) = \frac{4\pi}{3}R_c^3 \qquad \text{(Eq 1.6)}$$

We can now define the hypothetical shells at any time by:

$$R_{h,1} = \left(\frac{3}{4\pi}\sum_{j=1}^{i} V_{\mu,i}\right)^{1/3} \qquad \text{(Eq 1.7)}$$

$$R_{h,i} = \left(\frac{3}{4\pi}\sum_{j=1}^{i} V_j\right)^{1/3}; \quad i = 2,3,\ldots,N \qquad \text{(Eq 1.8)}$$

where $R_{h,o} = 0$

The radius of meso and microparticle at ith shell being:

$$R_{s,i} = \left(\frac{3}{4\pi}V_{s,i}\right)^{1/3} \qquad \text{(Eq 1.9)}$$

$$R_{\mu,i} = \left(\frac{3}{4\pi}V_{\mu,i}\right)^{1/3} \qquad \text{(Eq 1.10)}$$

The catalyst particles are assumed to be placed at the mid points of each hypothetical shell. Thus:

$$R_{1,i} = R_{h,i-1} + \left(\frac{1}{2}\right)\left(R_{h,i} - R_{h,i-1}\right); \quad i = 2,3\ldots,N \qquad \text{(Eq 1.11)}$$

Then the computational grid points are related to ($R_{1,i}$) by:

$$R_1 = 0 \qquad \text{(Eq 1.12)}$$

$$R_2 = R_c \qquad \text{(Eq 1.13)}$$

$$R_{i+1} = R_{1,i} + R_{s,i}; \quad i = 2,3,\ldots,N \qquad \text{(Eq 1.14)}$$

$$R_{N+2} = R_{h,N} \qquad \text{(Eq 1.15)}$$

The values of (Δr_i) to be used in the equation of Table 2 are given by:

$$\Delta r_i = R_{i+1} - R_i; \quad i = 1,2,\ldots,N+1 \qquad \text{(Eq 1.16)}$$

References

1. M. Malanga, O. Isogai, T. Yamada, S. Iwasaki, and M. Kuramoto, Ed., Historical Overview and Commercialization of Syndiotactic Polystyrene, *Syndiotactic Polystyrene*, John Wiley & Sons, Inc., New York, 2009, p 1–13. doi:10.1002/9780470557006.ch1
2. N. Ishihara, T. Seimiya, M. Kuramoto, and M. Uoi, Crystalline Syndiotactic Polystyrene, *Macromolecules*, 1986, **19**(9), p 2464–2465. doi:10.1021/ma00163a027
3. J.J. Han, H.W. Lee, W.J. Yoon, and K.Y. Choi, Rate and Molecular Weight Distribution Modeling of Syndiospecific Styrene Polymerization Over Silica-Supported Metallocene Catalyst, *Polymer*, 2007, **48**(22), p 6519–6531
4. J.J. Han, W.J. Yoon, H.W. Lee, and K.Y. Choi, Nascent Morphology of Syndiotactic Polystyrene Synthesized Over Silica-Supported Metallocene Catalyst, *Polymer*, 2008, **49**(19), p 4141–4149
5. H.W. Lee, J.S. Chung, and K.Y. Choi, Physical Transitions and Nascent Morphology of Syndiotactic Polystyrene in Slurry Polymerization with Embedded Cp*Ti$(OMe)_3$/Methyl Aluminoxane Catalyst, *Polymer*, 2005, **46**(14), p 5032–5039
6. S. Rahmani, R. Mohammadi, and A.A. Entezami, Comparison of Syndiotactic Polystyrene Morphology Obtained Via Heterogeneous and Homogeneous Polymerization with Metallocene Catalyst, *Macromol. Symp.*, 2008, **274**(1), p 43–48. doi:10.1002/masy.200851407
7. W.R. Schmeal and J.R. Street, Polymerization in Expanding Catalyst Particles, *AIChE J.*, 1971, **17**(5), p 1188–1197. doi:10.1002/aic.690170526
8. W.R. Schmeal and J.R. Street, Polymerization in Catalyst Particles: Calculation of Molecular Weight Distribution, *J. Polym. Sci.: Polym. Phys. Ed.*, 1972, **10**(11), p 2173–2187. doi:10.1002/pol.1972.180101106
9. E.J. Nagel, V.A. Kirillov, and W.H. Ray, Prediction of Molecular Weight Distributions for High-Density Polyolefins, *Ind. Eng. Chem. Prod. Res. Dev.*, 1980, **19**(3), p 372–379. doi:10.1021/i360075a016
10. D. Singh and R.P. Merrill, Molecular Weight Distribution of Polyethylene Produced by Ziegler-Natta Catalysts, *Macromolecules*, 1971, **4**(5), p 599–604. doi:10.1021/ma60023a017
11. R. Galvan and M. Tirrell, Orthogonal Collocation Applied to Analysis of Heterogeneous Ziegler-Natta Polymerization, *Comput. Chem. Eng.*, 1986, **10**(1), p 77–85
12. R. Galvan and M. Tirrell, Molecular Weight Distribution Predictions for Heterogeneous Ziegler-Natta Polymerization Using a Two-Site Model, *Chem. Eng. Sci.*, 1986, **41**(9), p 2385–2393
13. S. Floyd, K.Y. Choi, T.W. Taylor, and W.H. Ray, Polymerization of Olefins Through Heterogeneous Catalysis. III. Polymer Particle Modelling with an Analysis of Intraparticle Heat and Mass Transfer Effects, *J. Appl. Polym. Sci.*, 1986, **32**(1), p 2935–2960. doi:10.1002/app.1986.070320108

14. P. Varshney, D. Kunzru, and S.K. Gupta, A Multigrain Catalyst Model for Unifunctional Multicomponent Catalysts, *Chem. Eng. Res. Des.*, 2010, **88**, p 455–464
15. J.A. Debling and W.H. Ray, Heat and Mass Transfer Effects in Multistage Polymerization Processes: Impact Polypropylene, *Ind. Eng. Chem. Res.*, 1995, **34**(10), p 3466–3480. doi:10.1021/ie00037a035
16. P. Kittilsen and H.F. Svendsen, Three-Level Mass-Transfer Model for the Heterogeneous Polymerization of Olefins, *J. Appl. Polym. Sci.*, 2004, **91**(4), p 2158–2167. doi:10.1002/app.13338
17. S. Knoke, D. Ferrari, B. Tesche, and G. Fink, Microkinetic Videomicroscopic Analysis of Olefin Polymerization with a Supported Metallocene Catalyst, *Angew. Chem. Int. Ed.*, 2003, **42**(41), p 5090–5093. doi:10.1002/anie.200351582
18. F. Bonini, V. Fraaije, and G. Fink, Propylene Polymerization Through Supported Metallocene/MAO Catalysts: Kinetic Analysis and Modelling, *J. Polym. Sci., Part A: Polym. Chem.*, 1995, **33**(14), p 2393–2402. doi:10.1002/pola.1995.080331412
19. A. Alexiadis, C. Andes, D. Ferrari, F. Korber, K. Hauschild, M. Bochmann, and G. Fink, Mathematical Modeling of Homopolymerization on Supported Metallocene Catalysts, *Macromol. Mater. Eng.*, 2004, **289**(5), p 457–466. doi:10.1002/mame.200400011
20. S.R. Sultan, W.J.N. Fernando, and A.S. Sata, Multiscale Modeling of Syndiospecific Styrene Polymerization, *J. Polym. Res.*, 2012, **19**, p 9778
21. B.A. Finlayson, *Nonlinear Analysis in Chemical Engineering*, McGraw-Hill International Book Co., New York, 1980
22. T.K. Sherwood, R.L. Pigford, and C.R. Wilke, *Mass Transfer*, McGraw-Hill, Kogakusha, Tokyo, 1975
23. R.C. Reid, J.M. Prausnitz, and B.E. Poling, *The Properties of Gases and Liquids*, McGraw-Hill, New York, 1987
24. P. Sarkar and S.K. Gupta, Simulation of Propylene Polymerization: An Efficient Algorithm, *Polymer*, 1992, **33**(7), p 1477–1485
25. W.E. Ranz and W.R. Marshall, Jr., Evaporation from Drops. Part I, *Chem. Eng. Prog.*, 1952, **48**, p 141–146
26. E.L. Cussler, *Diffusion: Mass Transfer in Fluid Systems*, Cambridge University Press, Cambridge, 2009
27. P. Sarkar and S.K. Gupta, Modelling of Propylene Polymerization in an Isothermal Slurry Reactor, *Polymer*, 1991, **32**(15), p 2842–2852